A low cost, wide temperature range, and high energy density flexible quasi-solid-state zinc-ion hybrid supercapacitors enabled by sustainable cathode and electrolyte design

Guoshen Yang, Jialei Huang, Xuhao Wan, Yachao Zhu, Binbin Liu, Jiawei Wang, Pritesh Hiralal, Olivier Fontaine, Yuzheng Guo, Hang Zhou

▶ **To cite this version:**

Guoshen Yang, Jialei Huang, Xuhao Wan, Yachao Zhu, Binbin Liu, et al.. A low cost, wide temperature range, and high energy density flexible quasi-solid-state zinc-ion hybrid supercapacitors enabled by sustainable cathode and electrolyte design. Nano Energy, 2021, 90, pp.106500. 10.1016/j.nanoen.2021.106500 . hal-03413858

HAL Id: hal-03413858
https://hal.umontpellier.fr/hal-03413858

Submitted on 16 Oct 2023

HAL is a multi-disciplinary open access archive for the deposit and dissemination of scientific research documents, whether they are published or not. The documents may come from teaching and research institutions in France or abroad, or from public or private research centers.

L'archive ouverte pluridisciplinaire **HAL**, est destinée au dépôt et à la diffusion de documents scientifiques de niveau recherche, publiés ou non, émanant des établissements d'enseignement et de recherche français ou étrangers, des laboratoires publics ou privés.

Distributed under a Creative Commons Attribution - NonCommercial 4.0 International License

Version of Record: https://www.sciencedirect.com/science/article/pii/S2211285521007539
Manuscript_574a826351ed0746bb49b5e85ccdf75c

A low cost, wide temperature range, and high energy density flexible quasi-solid-state zinc-ion hybrid supercapacitors enabled by sustainable cathode and electrolyte design

Guoshen Yang [a], Jialei Huang [a], Xuhao Wan [b], Yachao Zhu [c], Binbin Liu [a], Jiawei Wang [a], Pritesh Hiralal [d], Olivier Fontaine*[c,e,f], Yuzheng Guo*[b], Hang Zhou*[a]

[a] School of Electronic and Computer Engineering, Peking University Shenzhen Graduate School, Shenzhen, 518055, China

[b] School of Electrical Engineering and Automation, Wuhan University, Wuhan, Hubei, 430072, China

[c] ICGM, Universsité de Montpellier, CNRS, Montpellier, France.

[d] Zinergy Shenzhen Ltd., Gangzhilong Science Park, Longhua, Shenzhen, 518109, China

[e] School of Energy Science and Engineering, Vidyasirimedhi Institute of Science and Technology (VISTEC), Rayong, 21210, Thailand.

[f] Institut Universitaire de France, 75005 Paris, France.

Corresponding Authors:

* Hang Zhou: zhouh81@pkusz.edu.cn.

* Yuzheng Guo: yguo@whu.edu.cn

* Olivier Fontaine: Olivier.fontaine@vistec.ac.th

© 2021 published by Elsevier. This manuscript is made available under the CC BY NC user license
https://creativecommons.org/licenses/by-nc/4.0/

ABSTRACT:

Zinc-ion hybrid supercapacitor (ZHSC), emerging as a promising energy storage device, bring together the benefits of the high power density of supercapacitors, the high energy density of batteries and the environmental and cost benefits of zinc-ion technology. However, the development of high energy density ZHSC working in a wide temperature range is still a challenge. The key to achieve this target is to develop the electrolyte with thermal stability and anti-freezing property which is compatible with the advanced cathode material. Herein, a natural biomass coconut shell derived activated carbon as cathode and cost-effective aqueous $Zn(ClO_4)_2$ as electrolyte, are applied in aqueous ZHSC. The fabricated aqueous ZHSC exhibits an outstanding high energy density of 190.3 Wh/kg at 89.8 W/kg. Furthermore, a robust flexible quasi-solid-state ZHSC device was constructed by using a cross-linked poly(vinyl alcohol)/montmorillonite/$Zn(ClO_4)_2$ gel electrolyte (PVA/MMT/$Zn(ClO_4)_2$), which shows superior electrochemical performance over a wide working temperature range. Experimental analysis and molecular dynamics simulations reveal that the $Zn(ClO_4)_2$ process faster ionic migration compared to other Zn-based salts and form more hydrogen bonds with H_2O, leading to a superior anti-freezing property. Our flexible device maintains the high energy storage capacities and excellent cycling stability over a wide temperature range from -50 °C to 80 °C, suggesting its great potential applications for energy storage applications in harsh environmental conditions.

KEYWORDS: Biomass activated carbon; zinc perchlorate; wide temperature range; high energy density; zinc-ion hybrid supercapacitors

1. INTRODUCTION

With the gradually exhausting fossil fuels and worsening global warming, it is urgent to develop energy storage devices to store electricity produced from renewable clean energy efficiently [1, 2]. As a new generation of energy storage devices, supercapacitor (SC) has gained enormous attention due to its high power density, high rate performance, and durability [3, 4]. Thanks to these advantages, SC is being successfully applied in portable electronics and hybrid electric vehicles [5]. Nonetheless, the relatively low energy density compared to the battery is hindering its widespread application [6, 7]. One practical strategy to improve on this is to fabricate a hybrid supercapacitor (HSC), which can have a high energy density (than capacitor) and high power density (than battery) with long cycle life. HSC represent an innovative candidate for next-generation superb energy storage [8-10]. Recently, the zinc-ion hybrid supercapacitor (ZHSC) has received attention, because of its high working voltage, material abundance, high safety, and low manufacture cost [11-13]. Generally, ZHSC is assembled by using carbon materials as the cathode, metallic zinc as the anode, and a zinc salt-containing solution as the electrolyte (such as $ZnSO_4$ and Zn $(CF_3SO_3)_2$) [11, 14]. The energy storage mechanism of ZHSC is electrolyte ion adsorption/desorption on the carbonaceous cathode, and Zn/Zn^{2+} stripping/plating on the zinc metal anode [15]. Considering that typically an excess amount of Zn is used as anode in ZHSC, the energy storage is commonly limited by the capacity of carbon cathode to adsorb/desorb electrolyte ions. Consequently, both cathode and electrolyte materials are highly significant in constructing high performance ZHSC. So far, many attempts about carbon cathode materials of ZHSC have been reported, for instance, activated carbon [11, 16, 17], carbon nanotubes

[9], graphene [18, 19], and porous carbon [10, 20], as summarized in Table S1. Despite these achievements, the energy density of ZHSC is still far from satisfactory. Furthermore, these carbon nanotubes and graphene always have disadvantages of complicated fabrication processes, high manufacture cost, and even environmental concerns. Therefore, it is highly desirable to exploit low-cost, eco-friendly and high-performance carbon materials. In this regard, the natural biomass-derived carbons such as coconut shell [21], rice husk [22], bamboo biochar [23], litchi shell [24], apricot shell [25], and peanut shell [26] have attracted much attention due to the large surface area, high porosity, cost-effective, and environment friendly. Among them, coconut shell derived carbons exhibit favorable electrochemical properties such as high specific capacity, good cycle ability, and availability, which is wildly used in electric double layer capacitor as electrode [27-29]. Besides, in economic terms, coconut shells are a natural fruit waste, and it has been frequently utilized as an adsorbent for water and gas purification due to its rich micropore molecular structure [30]. In this regard, activated carbon of coconut shell origin may be an ideal cathode material for constructing ZHSC.

Besides carbon cathode materials, the electrolyte also plays a pivotal role in the performance of the advanced ZHSC. Additionally, in some situations, energy storage devices need to be applied in harsh environmental conditions, especially in severe low and high temperature. Selecting the suitable electrolytes plays the critical role for designing ZHSC that can work in harsh environments. ZHSC with aqueous electrolytes has low cost, high safety, and environmental friendliness. So far, five typical Zn-based aqueous electrolytes including $ZnSO_4$, $Zn(CF_3SO_3)_2$, $Zn(CH_3COO)_2$, $ZnCl_2$, and $Zn(NO_3)_2$, have been reported in ZHSC [11,

19, 31]. Unfortunately, the freeze of aqueous electrolytes naturally suffers from severe ionic conduction capacity, thereby limit the low-temperature operation. Furthermore, Wang et al. reported the 1M $Zn(ClO_4)_2$ aqueous electrolyte in a Zn-V_2O_5 battery, which exhibited high anodic stability and excellent electrochemical performance at room temperature [32]. However, we are surprised to discover that the low concentration $Zn(ClO_4)_2$ aqueous has superior anti-freezing property, which is completely different from traditional freeze-resistant design strategy of "water-in-salt" electrolyte [33, 34] and cosolvents or additives [35, 36], as compared in Fig. S1. The low concentration $Zn(ClO_4)_2$ aqueous electrolyte is highly desired electrolyte for ZHSC with the wide working temperature range and low manufacturing cost.

In this work, an aqueous ZHSC with excellent electrochemical performance was assembled by using a natural coconut shell derived activated carbon as the cathode, $Zn(ClO_4)_2$ as the electrolyte, and electro-deposited Zn as the anode. The aqueous ZHSC exhibits an outstanding high energy density of 190.3 Wh/kg at 89.8 W/kg, which is the highest reported values for aqueous carbon-based ZHSC. Furthermore, a novel flexible quasi-solid-state ZHSC device was constructed based on cross-linked poly(vinyl alcohol)/montmorillonite/$Zn(ClO_4)_2$ (PVA/MMT/$Zn(ClO_4)_2$) gel electrolyte. This flexible quasi-solid-state ZHSC device delivers high energy storage capacities and great cycling stability over a wide temperature range from -50 to 80 °C, meaning that our flexible device opens a cost-effective and sustainable but efficient way for designing industrial zinc-ion hybrid supercapacitors and it has a promising application in harsh conditions for energy storage.

2. EXPERIMENTAL SECTION

2.1 Chemical reagents

$ZnSO_4 \cdot 7H_2O$ (AR, >99%), $Zn(CF_3SO_3)_2$ (AR, >99%), $Zn(ClO_4)_2 \cdot 6H_2O$ (AR, >99%), MMT, and PVA (Mw= ~145000) were purchased from Aladdin Chemical Reagent Co., Ltd.. Activated carbon (SSA: ~1150 m^2/g), hydroxylate multi-walled CNTs (SSA: ~233 m^2/g) and rGO (~700m^2/g) were purchased from China XFNANO Materials Tech Co., Ltd., and they were used for comparison.

2.2 Material preparation

Preparation of coconut shell activated carbon (CSAC): The CSAC was synthesized by a steam activation method. Briefly, the coconut shell was washed thoroughly with distilled water. Then the coconut shell is crushed, and the small particles (0.5 to 1.5 mm) were selected as experimental material. The collected samples were vacuum dried for 6h at 100 °C. This product was activated by heating at 900 °C while passing steam for 2 hours and then quenched with distilled water. Finally, the activated carbon was vacuum dried at 120 °C for 6 hours.

Preparation of coconut shell activated carbon (CSAC) cathode and Zn anode: The CSAC cathode slurry was prepared by following steps. First, 70 wt. % of CSAC powder, 20 wt. % of Super P, and 10 wt. % of Polytetrafluoroethylene (PTFE) were mixed and the mixture was dispersed in a certain of distilled water under magnetic stirring for 5h. Then, the slurry was uniformly coated on the carbon cloth and dried at 80 °C for 8 h. The mass loading of active material was around 2 mg/cm^2. The Zn anode was carried out by a constant current electrodeposition technique in an aqueous medium (0.4M $ZnSO_4 \cdot 7H_2O$ +0.9M Na_2SO_4 + 0.3

M H_3BO_3). An electrochemical cell with a carbon cloth was used as the working electrode and Pt plate as counter/reference electrode. The current density and time were -40 mA/cm^2 for 15 min at room temperature. The mass loading of zinc was ~8 mg/cm^2 (The surface morphology of the as-prepared Zn is shown in Fig. S2).

Preparation of poly(vinyl alcohol)/montmorillonite (PVA/MMT) *hydrogel electrolyte:* The preparation process of the PVA/MMT hydrogel electrolyte is similar to the previous report [37]. The hydrogel electrolyte was prepared as follows: 90 mg PVA powder and 10 mg MMT powder were added into 10 mL H_2O. The mixture solution was conducted at 80 °C under constant stirring until forming a jelly-like solution. Then, the jelly-like solution was transferred to a mould and the PVA/MMT membrane was easily peeled off after the vacuum drying for 24 h. Finally, the PVA/MMT hydrogel electrolyte was obtained after immersing into 3 M $Zn(ClO_4)_2$ solution for 30 min.

2.3 Structural characterization and computational details

The molecular structure of the samples was measured by Raman spectrometer (Raman, LabRAM HR800, Horiba Jobin Yvon S.A.S) and Fourier transform infrared spectrometer (FTIR, Bruker Vertex-70). The crystal phase of the samples was examined by X-ray diffraction (XRD, Bruker). The surface morphology of the samples was analyzed by field emission scanning electron microscopy (SEM, Zeiss Supra, Carl Zeiss) equipped with EDX analyzer. The morphological features of the samples were examined using transmission electron microscopy (TEM, JEM-3200FS, JEOL). The chemical composition of the products was analyzed using X-ray photoelectron spectroscopy (XPS, AXIS Ultra DLD, Kratos

Analytical Ltd.). The freezing point of the electrolyte was examined by the differential scanning calorimetry (DSC, DSC1, Mettler Toledo). The dynamic reaction coordinate (DRC) simulation, one of the molecular dynamics (MD) methods, is employed to investigate the properties of electrolyte aqueous in the study by MOPAC 2016 [38, 39]. The simulation temperature is set to 300 K, and the simulation lasts for 20 ns, with a 1 fs interval and total 1000 steps. The 'half-life' for loss of kinetic energy is 50 fs. Additionally, VMD3 (Visual Molecular Dynamics) is applied to build the model and study the RDF (Radial Distribution Function). The electrolytes are surrounded by a [60*60*60] Å water box [40].

2.4 Assembly of ZHSC devices

Aqueous and quasi-solid-state ZHSC devices were fabricated for cell performance evaluation by stacking the CSAC cathode and the electro-deposited Zn anode, in which aqueous 3 M $Zn(ClO_4)_2$ solution was used for aqueous ZHSC and the PVA/MMT/$Zn(ClO_4)_2$ hydrogel electrolyte for quasi-solid-state ZHSC devices. For aqueous ZHSC, the Zn anode and CSAC cathode were separated by a 50μm-thick fiberglass separator.

2.5 Electrochemical characterization

Cyclic voltammogram (CV), linear sweep voltammetry (LSV), galvanostatic charge-discharge (GCD), and electrochemical impedance spectroscopy (EIS) measurements were carried out on a commercial CHI660 electrochemical workstation (Shanghai CH Instrument Co., Ltd.). The EIS measurement was measured in the frequency range of 0.01-100kHz with an amplitude of 5 mV. The ionic conductivities of the aqueous and hydrogel electrolytes were measured by using EIS method. The ion conductivity was calculated from the Nyquist plot using the following equations:

$$\sigma = \frac{L}{R_s A}$$

Where σ (S/cm) represents the ion conductivity; L (cm) is interval distance between the two stainless steel electrodes; A (cm^2) is electrode contact area; R_s (Ω) is the electrolyte resistance, which was obtained from the intercept with the x-axis in Nyquist plots. All the electrochemical measurements were conducted under the constant applied temperature and humidity chamber at different temperatures (RHP-23, REALE). CV curves of Zn plating/stripping were measured using a three-electrode system consisting of stainless steel/Zn/Zn as working/counter/reference electrode.

3. RESULTS AND DISCUSSION

3.1 Structural study

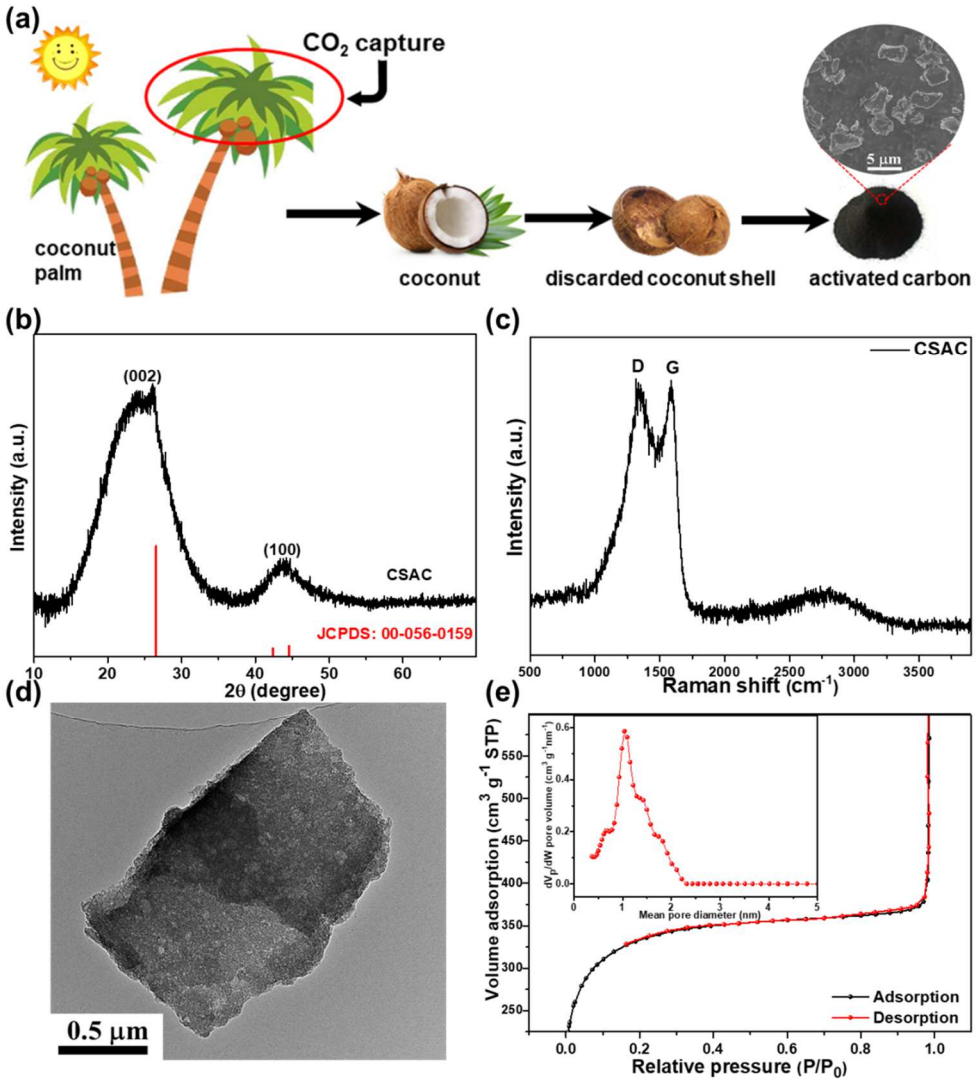

Fig. 1. (a) Schematic illustration of the coconut cycle of coconut, coconut shell, and biochar. (b, c) XRD and Raman spectra of CSAC. (d) TEM image of CSAC. (e) N_2 adsorption and desorption isotherms and pore size distribution of CSAC. (A color version of this figure can be viewed online.)

The energy density improvement and low manufacturing cost of ZHSCs are the main challenge to realize the future large-scale commercial applications. As carbonaceous materials are used as the cathode in ZHSC, so the carbon material with high surface area, sustainability and low cost is extremely important for commercial applications. Coconut palm is grown in more than 93 countries and is very prolific [41]. Coconut shell, as a source used to produce activated carbon, has the double advantage of low manufacturing cost and

sustainability. The optical and SEM image of the CSAC prepared in this work is illustrated in Fig. 1a. XRD and Raman were used to characterize the structure of as-prepared CSAC sample. As shown in Fig. 1b, the two broad diffraction peaks at 2θ values of around 25° and 43° are indexed as the (002) and (100) planes of graphite structure [42]. Raman spectra of CSAC are depicted in Fig. 1c, where two characteristic peaks at around 1340 cm^{-1} and 1588 cm^{-1} are the typical D and G bands, respectively. The intensity ratio of I_D/I_G bands can reflect the graphitic degree of the carbon materials. It is found that the CSAC has a higher I_D/I_G value (1.02) than the reported graphene oxide [43, 44], suggesting that it formed more defects in CSAC during the preparation process. The SEM (Fig. S3a) and TEM (Fig. 1d) images of the CSAC clearly seen that the carbonaceous materials with porous structure, which can facilitate the adsorption/desorption of electrolyte ions onto/into the sample surface to enhance the energy storage performance. ~~From the HRTEM image in Fig.S3b, the lattice fringes can be clearly observed. The interlayer spacings values of CSAC ($d_{(002)}$ = 0.366) are greater than the value of ideal graphite ($d_{(002)}$ = 0.335 nm) (JCPDS 00-056-0159), agreeing well with the above XRD analysis. The increased layer spacing is associated with a more disordered nature of the CSAC, which can facilitate the rapid penetration of electrolyte ion and therefore improving the energy storage properties [42].~~ EDX and XPS further characterized the chemical composition and elemental distribution of the CSAC. EDX mapping analysis (Fig. S3b) exhibits a homogeneous distribution of the elements (C, O, and N) in the CSAC. The full XPS spectrum of the as-synthesized sample (Fig. S3c) indicates about 90.76% C, 7.91% O, and 1.33% N in CASC. Nitrogen adsorption-desorption measurement was conducted to investigate the pore structures of as-prepared CSAC powder. As displayed in Fig. 1e, the

BET specific surface area of CSAC is 1260 m^2/g with the pore volume of 1.8 cm^3/g, which is larger than many reported CSAC [21, 27]. And the porosity is mostly concentrated around 1.03 nm, indicating a nano-sized porous structure of bulk CSAC. The larger specific surface area and nano-porous structure of CSAC can accelerates the kinetics of electrolyte ions and provides sufficient active sites for charge storage. All the above results prove the CSAC should be a promising cathode material for high energy density ZHSC.

3.2. Electrochemical performance of aqueous ZHSC device

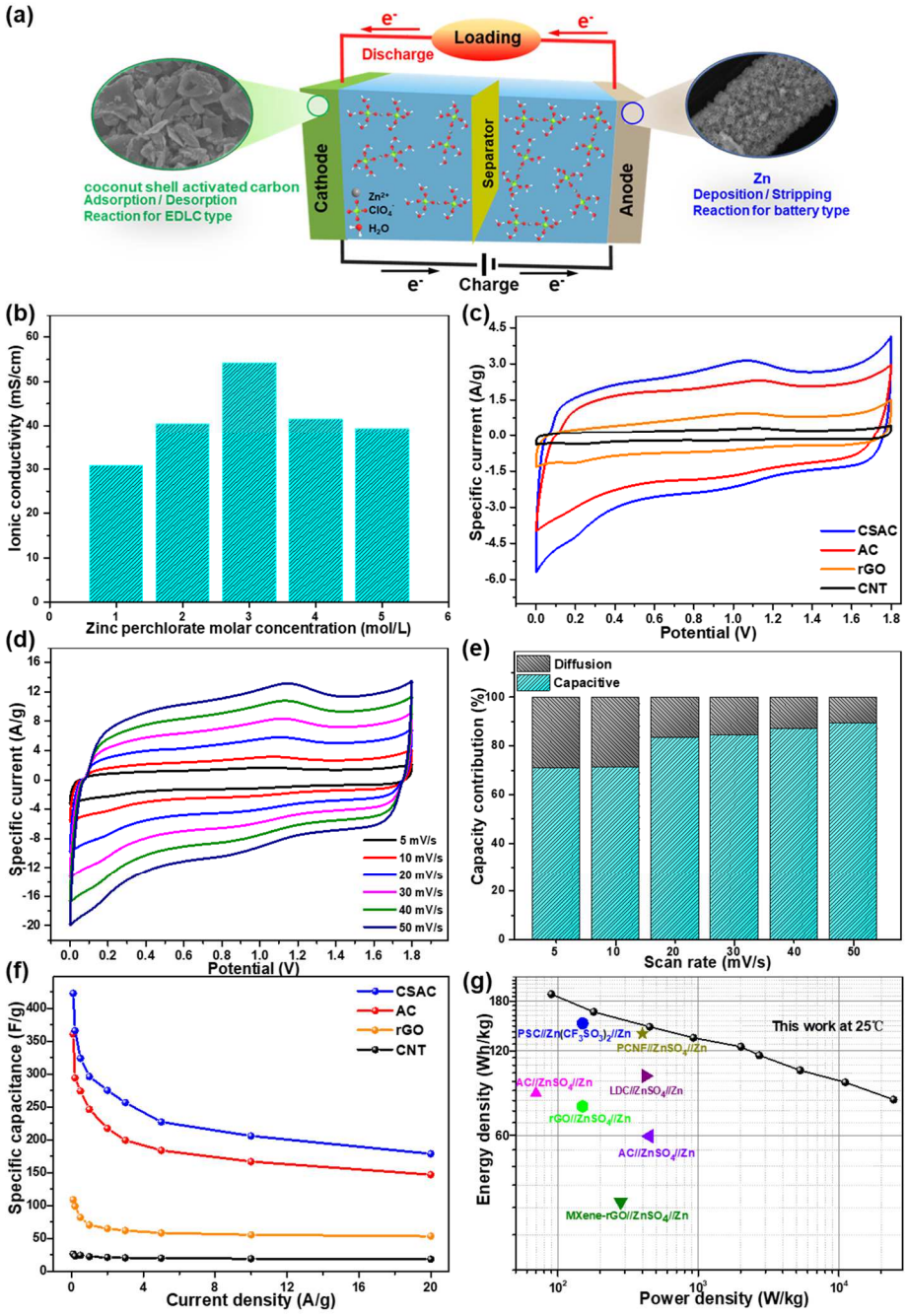

Fig. 2. Electrochemical performance of aqueous ZHSC device. (a) Schematic illustration of the CSAC//Zn$(ClO_4)_2$ (aq.)//Zn device. (b) Ionic conductivities of the zinc perchlorate electrolyte at different molar concentration. (c) CV curves of ZHSC devices with different carbon cathode at 10 mV/s. (d) CV curves of the ZHSC device with CSAC cathode at different scan rates. (e) The capacitive and diffusion contribution ratios to the total capacity of ZHSC at different scan rates. (f) Specific capacitance values of ZHSC devices with different carbon cathode at various current densities. (g) Ragone plots of

CSAC//$Zn(ClO_4)_2$ (aq.)//Zn device in comparison to other ZHSC at 25 °C. (A colour version of this figure can be viewed online.).

To assess the performance of as-prepared CSAC for zinc-ion energy storage in realistic applications, an aqueous CSAC//$Zn(ClO_4)_2$ (aq.)//Zn device was manufactured, as illustrated in Fig. 2a. Due to the hybrid of battery-type Zn anode and EDLC-type CSAS cathode, the assembled ZHSC can store charges through reversible Zn^{2+} ions stripping/deposition onto the Zn anode and electrolyte anion adsorption/desorption onto CSAS cathode [10]. Thus, improved power and energy densities can be fulfilled in this device. The ionic conductivity of $Zn(ClO_4)_2$ electrolyte at different molar concentrations was first studied by calculating through EIS (Fig. S4a) and the values of ionic conductivity are represented in Fig. 2b. With raising the concentration, the ionic conductivity of $Zn(ClO_4)_2$ aqueous solution increases first and then decreases under room temperature. Notably, the 3M $Zn(ClO_4)_2$ aqueous solution has the highest ionic conductivity (Fig. 2b). While the concentration increases to higher than 3M, the ionic conductivity of the electrolyte decreases. It is probably due to the increase of viscosity with raising the concentration [45-46]. The high viscosity will slower the transport of ions in electrolyte and decrease the ionic conductivity [47, 48]. Thus, the 3M $Zn(ClO_4)_2$ with the optimal ionic conductivity was selected as the electrolyte for fabricating aqueous ZHSC in this work. Meanwhile, the electrochemical stability window of electrolytes was also verified by applying LSV measurement. As shown in Fig. S4b, the $Zn(ClO_4)_2$ electrolyte has a high electrochemical stability window of 2.5 V, which is capable to perform almost all aqueous ZHSC devices. To confirm the practical electrochemical stability window of the assembled aqueous ZHSC, the CV measurements were performed with various potential

ranges (Fig. S4c). In detail, the CV curve within 0 - 1.8 V has negligible distortion, while an apparent polarization phenomenon is observed with extending the window voltage to 1.9 V. Consequently, the suitable potential window of ZHSC was 0 to 1.8 V. In addition, to highlight the performance of ZHSC, other carbon-based cathodes (commercial AC, rGO, and CNT) were also applied in ZHSC for comparison. Fig. 2c displays the CV curves at 10 mV/s and Fig. S4d exhibits the GCD curves at 0.5A/g of corresponding ZHSC. Notably, CSAC//$Zn(ClO_4)_2$ (aq.)//Zn has the largest enclosed area and longest discharge time, indicating that the as-prepared CSAC cathode has an advanced electrochemical performance in ZHSC. Their specific surface areas are shown in Fig. S5, indicating that the larger surface area of porous CSAC materials can enhance the energy storage capacity. Fig. 2d displays the CV curves of CSAC//$Zn(ClO_4)_2$ (aq.)//Zn at various scan rates. It is exhibited that a rectangular shape is still kept at 50 mV/s scan rate, implying the excellent kinetics and highly rechargeable feature [11]. Unlike the regular rectangular CV shape observed from typical EDLC [49], the formation of such curves for CSAC//$Zn(ClO_4)_2$ (aq.)//Zn can be ascribed to both diffusion and capacitive processes. To further analyze the kinetics over charging-discharging process, the contribution of diffusion/capacitive behavior can be calculated by the following equations [50]:

$$i(V) = i_{cap} + \ i_{diff} = k_1 v + k_2 v^{1/2} \quad (1)$$

or

$$\frac{i(V)}{v^{1/2}} = k_1 v^{1/2} + k_2 \quad (2)$$

Based on Equation (1) and (2), the values of k_1 and k_2 can be obtained from the curve plotting the relationship curves of $i(V)/v^{1/2}$ and $v^{1/2}$, and thus the charge storage contributions of diffusion/capacitive can be assessed. Thus, the overall capacitance Q can be separated into the capacitance charge storage Q_{cap}deriive process and bulk charge storage Q_{bulk} which depends upon a diffusion-controlled process as shown in the following equation (3).

$$Q_{bulk} = Q_{cap} + \ Q_{diff} \quad (3)$$

As shown in Fig. S6, the capacitive contribution (the shaded area) is calculated to be almost 83% of the total charge stored at 20 mV/s for CSAC//$Zn(ClO_4)_2$ (aq.)//Zn. Moreover, in Fig. 2e, the capacitance contributions are 70 %, 71 %, 83 %, 84 %, 87 %, and 89 % from 5 to 50 mV/s, indicating the capacitive contribution is dominant during the charge storage even at a low scan rate, which proves that it has high kinetics and high rate performance in CSAC//$Zn(ClO_4)_2$ (aq.)//Zn. As presented in Fig. 2f, CSAC/$Zn(ClO_4)_2$ (aq.)//Zn delivers excellent rate properties of 423.5 to 178.8 F/g at current densities from 0.1 to 20 A/g, much higher than that of AC//$Zn(ClO_4)_2$ (aq.)//Zn (364.4 to 147.2 F/g), rGO//$Zn(ClO_4)_2$ (aq.)//Zn (109.0 to 53.5 F/g) and CNT//$Zn(ClO_4)_2$ (aq.)//Zn (26.3 to 18.5 F/g) under the same measurements. The compelling capacitance and rate performance of our CSAC/$Zn(ClO_4)_2$ (aq.)//Zn are superior to many recently reported work on carbon-based ZHSC, as summarized in Table S2. The results show that our device possesses superior capacitance, good rate capability, and high energy density. The superior electrochemical properties of this device can be ascribed to the high ionic conductivity of $Zn(ClO_4)_2$ electrolyte and the CSAC cathode with a larger specific surface area and nano-porous structure. To evaluate the performance of the ZHSC device in terms of energy and power density, the Ragone plot is shown in Fig. 2g.

The CSAC//$Zn(ClO_4)_2$ (aq.)//Zn device can offer an ultra-high energy density of 190.3 Wh/kg at 89.8 W/kg and it still can retain 80.5 Wh/kg at an ultra-high power density 24.5 kW/kg, for now, which is highest energy densities value in previously reported aqueous ZHSC work [10, 11, 18, 20, 51-53].

3.3 Electrochemical properties of quasi-solid-state ZHSC devices

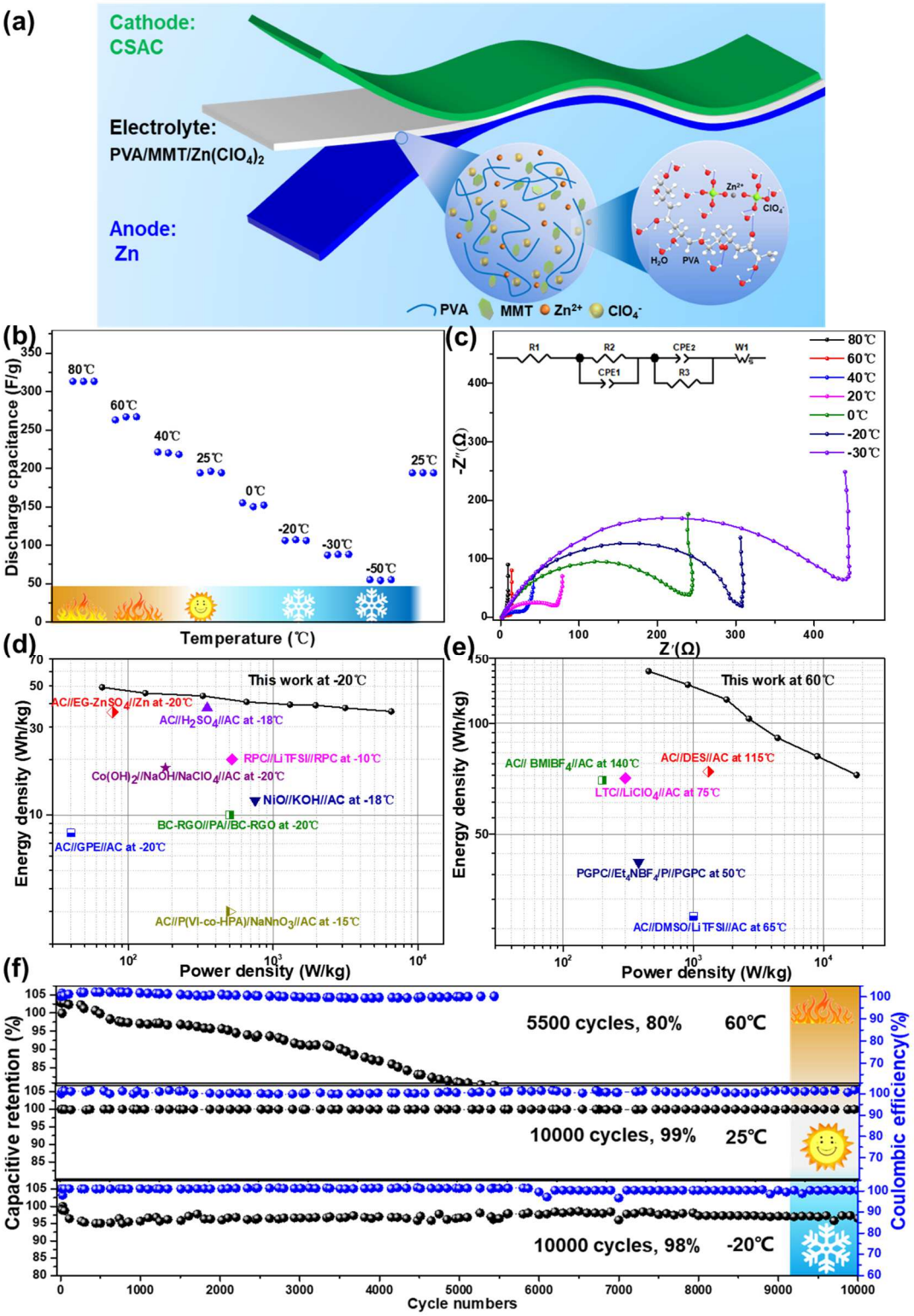

Fig. 3. Electrochemical properties of quasi-solid-state ZHSC device. (a) Schematics of quasi-solid-state CSAC//PVA/MMT/$Zn(ClO_4)_2$ (gel)//Zn. (b) Specific capacitance at different temperature with a current density of 0.5 A/g. (c) Nyquist plots at different temperature. (d, e) Ragone plot of the quasi-solid-state

ZHSC device in comparison to other SCs at 60 °C and -20 °C. (f) Cycling performance of the quasi-solid-state ZHSC device at 5A/g under different temperatures.

As described, the satisfactory electrochemical performance of aqueous ZHSC was achieved. It should be noted, however, that $Zn(ClO_4)_2$ belongs to the class of Lewis acids [54]. Although aqueous electrolyte can provide high ionic conductivity, 3M $Zn(ClO_4)_2$ aqueous solution displays strong acidity, which may cause the risk of leakage and safety in practical application, especially for the application of flexible wearable electronics. Preparation of gel electrolyte can effectively solve this problem. Based on this consideration, a quasi-solid-state CSAC//PVA/MMT/$Zn(ClO_4)_2$ (gel)//Zn device was further manufactured, where CSAC, PVA/MMT/$Zn(ClO_4)_2$, and Zn respectively served as cathode, separator/electrolyte, and anode (Fig. 3a). Fig. S7a shows the GCD curves of the quasi-solid-state ZHSC device at various current densities. The specific capacitance of the quasi-solid-state ZHSC is 206 F/g at 0.5A/g and the specific capacitance retentions can still retain 70% at 20A/g (Fig. S7b), suggesting its excellent rate capability. The operating temperature range is also a critical parameter for flexible energy storage devices, especially for the device needs to work in harsh environments. Thus, thermal performance is also one of the critical elements for the energy storage device. First, the thermal behavior of PVA/MMT/$Zn(ClO_4)_2$ gel electrolyte was analyzed. The result in Fig. S8a reveals that the endothermic peak is hard to be observed at the low temperature range, which suggests that the crystallization is strongly suppressed. It has a sharp exothermic peak at around 95 °C due to water vaporization. In Fig. S8b, the peak at 84 °C represents the glass transition temperature of PVA [55]. The results reveal the PVA/MMT/$Zn(ClO_4)_2$ gel possesses a larger working temperature window (-60~80 °C).

Depended on the thermal performance, the electrochemical measurements have carried out under a series of working temperatures. Fig. 3b shows the specific capacitance variation with changing working temperatures of the quasi-solid-state ZHSC. The specific capacitance of the device increases almost linearly with the temperature. The ZHSC displays around 303 F/g at 80 °C, which is about 195% capacitance retention compared to that at 25 °C. Furthermore, the ZHSC still has approximate 110 F/g at -20 °C, which is almost 54% capacity retention compared to that at 25 °C. More significantly, from 25 to -50 °C, the ZHSC can still maintain a high capacitance retention of 26.5%. It is worth to note that this is achieved without any anti-freezing agent. EIS measurement was employed to further explore the electrochemical behavior of the ZHSC with varying working temperatures, and the Nyquist plots are shown in Fig. 3c. All the nearly vertical lines in the low-frequency region also suggest the ZHSC have the ideal capacitive behavior at different working temperature, proving the above dominant capacitive contribution during the charging-discharging process.

Moreover, it is clear to see that the equivalent serial internal resistance (R_s), charge-transfer resistance (R_{ct}), and Warburg resistance (Z_w) vary significantly with the change of the test temperature. The inset in Fig. 3c is the equivalent circuit model, and the relative parameters are summarized in Table 1. With decreasing the ambient temperature from 80 to -30 °C, the R_s, R_{ct}, and Z_w show an increasing tendency. It is highlighted that the electrochemical performance has a strong effect on the electrolyte. With the decrease of working temperature, the mobility of $Zn(ClO_4)_2$ in PVA/MMT decreases, which leads to the decrease of ionic conductivity. The reduced ionic conductivity caused the increase of R_s. The kinetics of active materials for Zn^{2+}ions de/intercalation and electrolyte ion

adsorption/desorption decrease significantly with reducing temperature, which will result in an increased R_{ct}.

Table 1 R_e, R_{ct}, and Z_W parameters of ZHSC obtained from the Nyquist plot fitting.

Temperature (° C)	R_s (Ω)	R_{ct} (Ω)	Z_w (Ω/s$^{1/2}$)
-30	2.67	448.10	219.12
-20	2.48	315.60	158.05
0	1.93	245.40	104.02
20	1.75	77.05	78.20
40	1.63	34.91	41.19
60	1.55	11.58	15.60
80	1.34	4.06	10.14

Ragone plots of quasi-solid-state ZHSC devices are derived to assess the ZHSC device's output in terms of energy and power density. Remarkably, our quasi-solid-state ZHSC device delivers an outstanding energy density of 49.1Wh/kg and an excellent power density of 6.5 kW/kg under -20 °C (Fig. 3d), which is significantly superior to previous reported carbon-based hybrid devices with anti-freezing property [35, 56-62]. On the other side, the quasi-solid-state ZHSC device also delivers a superior energy density of 138.6 Wh/kg and an excellent power density of 18 kW/kg under 60 °C (Fig. 3e), which is also significantly superior to other advanced supercapacitor with the high temperature application [63-67]. Additionally, the cycling stability of the quasi-solid-state ZHSC device was evaluated by the charge-discharge process at 5 A/g. As shown in Fig 3f, over 10000 cycles, the specific capacitance retentions of ZHSC are 99% at 25 °C and 98% at -20 °C, respectively. The results uncover that the quasi-solid-state ZHSC device is stable to charge/discharge under a room temperature and even ultra-low temperature. Meanwhile, at the high temperature 60 °C,

the specific capacitance can retention 80% after 5500 cycles. The capacitance retention decreases with the cycles, which mainly resulting from the water evaporated caused ion diffusion of the hydrogel electrolyte to decrease little by little (see Supporting Information Fig. S9, Fig. S10 and Fig. S11 for details) [68]. It is worth noting that when the operating temperature of the quasi-solid-state ZHSC is further increased, the capacitance fading rate of the ZHSC is also increased. As shown in Fig. S12, although the quasi-solid-state ZHSC can work, the cycle stability is poor under 80 °C. In addition, it is found that it can work well again after resting at room temperature for 2h, which may relate to the PVA become glassy state again at room temperature.

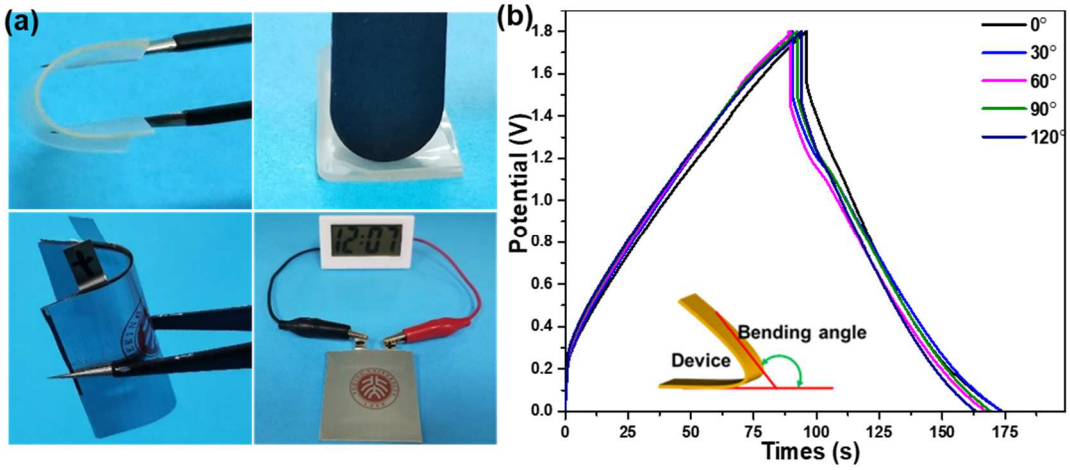

Fig. 4. (a) Photographs of the flexible PVA/MMT membranes and ZHSC device. (b) GCD curves under different flexible conditions.

For the flexible quasi-solid-state ZHSC devices, besides the flexible CSAC cathode and zinc anode, the flexibility of the PVA/MMT gel decides whether it can be used as power supply for wearable electronic devices. Optical images of PVA/MMT hydrogel and flexible ZHSC device are shown in Fig. 4a. The PVA/MMT hydrogel shows good flexibility with very thin and bendable. Because of the flexibility of the PVA/MMT hydrogel and electrodes,

the assembled solid state ZHSC also demonstrates excellent flexibility. To perform an evaluation of the mechanical property in its operational condition, the quasi-solid-state ZHSC device was bend at different angles (from 0° to 120°) and the corresponding GCD curves were measured in Fig. 4b. It depicts that the electrochemical performance can almost remain with varying bending angles, meaning the admirable mechanical flexibility of the quasi-solid-state ZHS device. To verify its practical application, the assembled flexible device was used to light an electric desktop clock after being charged to 1.8 V, indicating its considerable potential in renewable energy storage.

3.4 Mechanism research of ZHSC device achieving superior electrochemical performance

As mentioned above, the CSAC/$Zn(ClO_4)_2$ (aq.)//Zn device achieved enhanced capacitance, good rate performance, and outstanding energy density, which can surpass many other carbon-based zinc-ion hybrid devices. One of the reasons for the enhanced electrochemical performance of CSAC/$Zn(ClO_4)_2$ (aq.)//Zn could be ascribed to the CSAC cathode. The CSAC cathode could exhibit fast dynamics during the electrochemical process. It exposes more electroactive sites for energy storage, which was attributed to its high specific surface area and nano-pore structure. In addition, compared with other carbon-based ZHSC devices, zinc perchlorate salt is used as an electrolyte for the first time in ZHSC. Therefore, the second reason may be ascribed to the use of zinc perchlorate as electrolyte. To verify our thoughts, we tested the CV and GCD measurements in ZHSC devices with different zinc salts ($ZnSO_4$, $Zn(CF_3SO_3)_2$), but using the same cathode and anode. In Fig. S13, the larger CV integral area and longer discharge time demonstrate that the device with

$Zn(ClO_4)_2$ electrolyte can obtain more excellent electrochemical performance. Therefore, the enhanced electrochemical performance should be related to the stripping/plating reaction rate of Zn anode and the ion diffusion rate of electrolyte. The deposition/dissolution efficiency of Zn anode in three electrolytes was investigated via using a CV test. Fig. S14a-c show the comparison of the 2nd and 20th CV curves in three electrolytes, which reflects the electrochemical stripping/plating process of Zn. The details are displayed in Table S3, where I_{PC} is the Zn dissolution peak current corresponding to the 2nd to the 20th cycles, respectively. The purpose of Fig. S14d is to depict the average of the CV measurement data recorded over the potential range -0.25 to +0.5 V during 19 cycles (from the 2nd cycle to the 20th cycle) in three electrolytes. It discovers that I_{PC} in the curve of $Zn(ClO_4)_2$ is much higher than those in the curves of the $ZnSO_4$ and $Zn(CF_3SO_3)_2$ electrolytes. It indicates that using $Zn(ClO_4)_2$ electrolyte can effectively improve the reaction rate of Zn anodic dissolution. Furthermore, as shown in Fig. S14a-c and Table S3, using $Zn(ClO_4)_2$ electrolyte provides the lowest peak current differences between the 2nd and 20th cycles, meaning its highly reversible electrochemical stripping/plating process of Zn. These inspired results manifest that the existence of ClO_4^- could lead to faster dynamics during the electrochemical process, which could attribute to its high ionic conductivity.

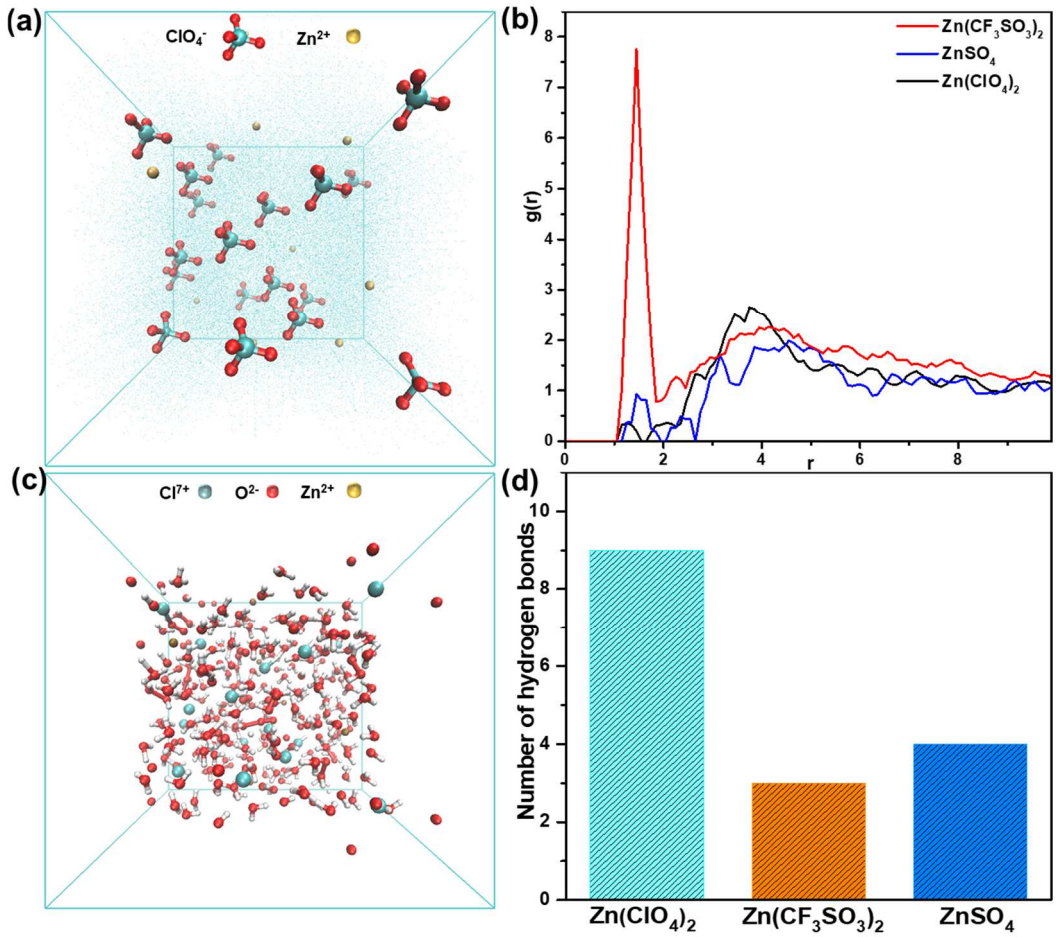

Fig. 5. (a) Molecular dynamics simulation snapshot of $Zn(ClO_4)_2$ electrolyte. (b) Radial distribution functions of $Zn(ClO_4)_2$, $ZnSO_4$, and $Zn(CF_3SO_3)_2$, respectively. (c) The snapshot of the MD simulation of $Zn(ClO_4)_2$ and water. (d) Averaged hydrogen bonds numbers for $Zn(ClO_4)_2$, $ZnSO_4$, and $Zn(CF_3SO_3)_2$ systems.

To make a deep comprehension on the ionic conductivity of the different zinc salts electrolyte, molecular dynamics (MD) simulations were performed (Fig. 5a, Fig. S15a, and Fig. S15b). The diffusion coefficients of different Zn-based salts were analyzed by the radial distribution functions (RDF) (Fig. 5b). For the $Zn(CF_3SO_3)_2$ electrolyte, the main peak position is near 1.45 A, which indicates $Zn(CF_3SO_3)_2$ has a low diffusion coefficient. For the $Zn(ClO_4)_2$ and $ZnSO_4$ electrolyte, they have similar radial distribution with average diffusion distribution, which should in principle leads to higher diffusion coefficient than that of the

$Zn(CF_3SO_3)_2$. As for $ZnSO_4$ electrolyte, the number of SO_4^{2-} anions is less than half of ClO_4^- under the same concentration. Therefore, the diffusion of $Zn(ClO_4)_2$ should be more significant than that of $ZnSO_4$ and $Zn(CF_3SO_3)_2$ electrolyte. Therefore, the higher diffusion coefficient of $Zn(ClO_4)_2$ result in a faster ion diffusion rate in aqueous solution, which can accelerate the electrochemical reaction.

Furthermore, the flexible quasi-solid-state ZHSC device also displays excellent electrochemical performance under a wide temperature range from -50 to 80 °C. The constructed PVA/MMT/$Zn(ClO_4)_2$ gel electrolyte plays a key role for wide working temperature flexible ZHSC due to its thermally stable and anti-freezing capability. As shown in Fig. S16, the PVA/MMT membrane is the porous structure, which can form ion transport paths in the hydrogel electrolyte system and further enhancing its ionic conductivity under electrochemical processes. Moreover, MMT materials can promote the thermal stability and facilitate ionic conductivity of the hydrogel electrolyte, which is confirmed by TGA technique and electrochemical measurements (see Supporting Information Fig. S17 and Fig. S18 for details). Our experimental results are also similar to reported results by previous literature [37, 69, 70]. Therefore, the hydrogel has high ion transport efficiency and thermal stability. Usually, the hydrogel electrolytes without any anti-freezing agent freeze easily under subzero temperatures, resulting in deteriorated ionic conductivity. Surprisingly, the $Zn(ClO_4)_2$ aqueous electrolyte is found to have superior anti-freezing performance (Fig. S19) and excellent ionic conductivity (Fig. S20) even at -50 °C. It is worth mentioning that the $Zn(ClO_4)_2$ has excellent anti-freezing properties, which can be achieved under the low concentration zinc-based salt and without any anti-freezing agent. This is a cost-effective new

way of making freeze-resistant electrolyte. In order to understand the mechanisms behind these phenomena, mechanism analysis was also conducted. The anti-freezing performance of $Zn(ClO_4)_2$ aqueous electrolyte should be related to the interaction of solute $Zn(ClO_4)_2$ with solvent water molecules to block the formation of the ordered hydrogen bond network among water molecules. The condition of hydrogen bonds between the $Zn(ClO_4)_2$ electrolyte and water molecules is investigated by analyzing the above simulation results (Fig. 5c), and we also compared with $ZnSO_4$ and $Zn(CF_3SO_3)_2$ electrolyte under the same condition (Fig. S15c, S15d). It is found that many hydrogen bonds are formed between solute zinc-based salts and solvent water molecules. Further observation found that most hydrogen bonds are formed between the hydrogen atoms of water molecules and the anions of the zinc-based salts. As for $ZnSO_4$ and $Zn(CF_3SO_3)_2$ aqueous electrolyte, the new hydrogen bonds were observed between hydrogen atoms of water molecules and the oxygen atom of SO_4^{2-} and $CF_3SO_3^-$. Interestingly, for $Zn(ClO_4)_2$ aqueous electrolyte, the new hydrogen bonds were not only observed between hydrogen atoms of water molecules and the oxygen atom of ClO_4^-, but also between hydrogen atoms of water molecules and chlorine atom of ClO_4^-, which leads to more hydrogen bonds in $Zn(ClO_4)_2$ than in $Zn(CF_3SO_3)_2$ and $ZnSO_4$. The formation of new hydrogen bonds in aqueous $Zn(ClO_4)_2$ solution was also confirmed by FTIR. Usually, the absorption band of H-O-H bending vibration of liquid water is at 1640 cm^{-1} [71]. However, the FTIR spectrum in Fig. S21 indicates a slight red shift in the bending vibration of H_2O at around 1630 cm^{-1} as the $Zn(ClO_4)_2$ concentration increases, implying hydrogen bond between $Zn(ClO_4)_2$ and H_2O. As shown in Fig. 5d, the ratio of the number of hydrogen bond for the $Zn(ClO_4)_2$, $Zn(CF_3SO_3)_2$ and $ZnSO_4$ is about 9:3:4. A large number of hydrogen bonds

between solute $Zn(ClO_4)_2$ and solvent water molecules can effectively prevent the formation of an ordered hydrogen bond network among water molecules, thus reducing the freezing point of the aqueous electrolyte.

4. CONCLUSIONS

In this work, an advanced ZHSC with superior capacitance and anti-freezing performances has been successfully assembled. The pores coconut shell derived activated carbon accelerates the kinetics of electrolyte ions and provides sufficient active sites for charge storage. The high ionic conductivity of $Zn(ClO_4)_2$ promotes fast dynamics during the electrochemical process and improve the capacitance performance, with excellent anti-freezing performance. When tested in aqueous electrolyte, the ZHSC device shows an ultra-high specific capacitance of 423.5 F/g and an outstanding high energy density of 190.3 Wh/kg at 89.8 W/kg. Besides, an anti-freezing and thermally stable PVA/MMT/$Zn(ClO_4)_2$ hydrogel electrolyte are used to prepare flexible quasi-solid-state ZHSC. The manufactured flexible device displays high energy density without compromising power density and excellent cycling stability under a wide temperature range, from -50 to 80 °C, which discloses the excellent anti-freezing property. Our ZHSC device could bridge the energy density gap between battery and supercapacitor for energy storage. It is worth mentioning that the CSAC has high surface area and low cost, and the low concentration $Zn(ClO_4)_2$ has excellent anti-freezing property without any anti-freezing agent, which has the potential realizing mass production for commercial applications for high-performance ZHSC. This work presented here also presents an encouraging pathway via sustainable cathode and

electrolyte design pathway towards high energy density flexible energy storage devices with excellent flexibility as well as wide operating temperature range.

CRediT authorship contribution statement

Guoshen Yang: Conceptualization, Investigation, Data curation, Writing-original draft. **Jialei Huang:** Conceptualization, Investigation. **Xuhao Wan:** Formal analysis, dynamic reaction coordinate (DRC) simulation. **Yachao Zhu:** Formal analysis, Investigation. **Binbin Liu:** Formal analysis. **Jiawei Wang:** Formal analysis. **Pritesh Hiralal:** Investigation. **Olivier Fontaine:** Visualization, Validation, Writing - review & editing. **Yuzheng Gu:** Resources, Writing - review & editing. **Hang Zhou:** Funding acquisition, Resources, Supervision, Visualization, Validation, Writing - review & editing.

Declaration of competing interest

The authors declare that they have no known competing financial interests or personal relationships that could have appeared to influence

Acknowledgments

This work is supported by Shenzhen Science and Technology Innovation Committee (No. JCYJ20190806145609284, No. GJHZ20190820091203667), Guangdong Basic and Applied Basic Research Foundation (2020A1515010716), and the Guangdong Introducing Innovative and Entrepreneurial Teams Program (2019ZT08Z656). P. Hiralal would like to acknowledge Shenzhen Science and Technology Program (KQTD20190929172522248). Technical support from GROUPSTARS CHEMICAL (YUNNAN) CHINA L.L.C. is acknowledged.

REFERENCES

[1] P. He, Q. Chen, M. Yan, X. Xu, L. Zhou, L. Mai, C.W. Nan, EnergyChem, 1 (2019) 100022.

[2] Y. Liu, T. Lv, H. Wang, X. T. Guo, C. S. Liu, H. Pang, Chemical Engineering Journal, 417 (2021) 128408.

[3] L. Chen, Y. Lu, L. Yu, X.W. Lou, Energy & Environmental Science, 10 (2017) 1777-1783.

[4] P. Simon, Y. Gogotsi, B. Dunn, Science, 343 (2014) 1210.

[5] Y. Da, J. Liu, L. Zhou, X. Zhu, X. Chen, L. Fu, Advanced Materials, 31 (2019) 1802793.

[6] G. Wang, H. Wang, X. Lu, Y. Ling, M. Yu, T. Zhai, Y. Tong, Y. Li, Advanced Materials, 26 (2014) 2676-2682.

[7] Z. Liu, H. Li, M. Zhu, Y. Huang, Z. Tang, Z. Pei, Z. Wang, Z. Shi, J. Liu, Y. Huang, C. Zhi, Nano Energy, 44 (2018) 164-173.

[8] W. Zuo, R. Li, C. Zhou, Y. Li, J. Xia, J. Liu, Advanced Science, 4 (2017) 1600539.

[9] G. Sun, H. Yang, G. Zhang, J. Gao, X. Jin, Y. Zhao, L. Jiang, L. Qu, Energy & Environmental Science, 11 (2018) 3367-3374.

[10] Y. Lu, Z. Li, Z. Bai, H. Mi, C. Ji, H. Pang, C. Yu, J. Qiu, Nano Energy, 66 (2019) 104132.

[11] L. Dong, X. Ma, Y. Li, L. Zhao, W. Liu, J. Cheng, C. Xu, B. Li, Q.-H. Yang, F. Kang, Energy Storage Materials, 13 (2018) 96-102.

[12] T. Lv, Y. Liu, H. Wang, S. Yang, C. Liu, H. Pang, Chemical Engineering Journal, 411 (2021) 128533.

[13] L. Hu, P. Xiao, L. Xue, H. Li and T. Zhai, EnergyChem, 3 (2021) 100052.

[14] J. Zheng, Q. Zhao, T. Tang, J. Yin, C.D. Quilty, G.D. Renderos, X. Liu, Y. Deng, L. Wang, D.C. Bock, C. Jaye, D. Zhang, E.S. Takeuchi, K.J. Takeuchi, A.C. Marschilok, L.A. Archer, Science, 366 (2019) 645-648.

[15] L. Dong, W. Yang, W. Yang, Y. Li, W. Wu, G. Wang, Journal of Materials Chemistry A, 7 (2019) 13810-13832.

[16] M. Chen, J. Chen, W. Zhou, J. Xu, C.-P. Wong, Journal of Materials Chemistry A, 7 (2019) 26524-26532.

[17] L. Han, H. Huang, X. Fu, J. Li, Z. Yang, X. Liu, L. Pan, M. Xu, Chemical Engineering Journal, 392 (2020) 123733.

[18] Q. Wang, S. Wang, X. Guo, L. Ruan, N. Wei, Y. Ma, J. Li, M. Wang, W. Li, W. Zeng, Advanced Electronic Materials, 5 (2019) 1900537.

[19] S. Wu, Y. Chen, T. Jiao, J. Zhou, J. Cheng, B. Liu, S. Yang, K. Zhang, W. Zhang, Advanced Energy Materials, 9 (2019) 1902915.

[20] Z. Pan, Z. Lu, L. Xu, D. Wang, Applied Surface Science, 510 (2020) 145384.

[21] Y.J. Hwang, S.K. Jeong, J.S. Shin, K.S. Nahm, A.M. Stephan, Journal of Alloys and Compounds, 448 (2008) 141-147.

[22] R. Pode, Renewable and Sustainable Energy Reviews, 53 (2016) 1468-1485.

[23] X. Gu, C. Lai, F. Liu, W. Yang, Y. Hou, S. Zhang, Journal of Materials Chemistry A, 3 (2015) 9502-9509.

[24] Z. Sun, S. Wang, L. Yan, M. Xiao, D. Han, Y. Meng, Journal of Power Sources, 324

(2016) 547-555.
[25] B. Janković, N. Manić, V. Dodevski, I. Radović, M. Pijović, Đ. Katnić, G. Tasić, Journal of Cleaner Production, 236 (2019) 117614.
[26] J. Ding, H. Wang, Z. Li, K. Cui, D. Karpuzov, X. Tan, A. Kohandehghan, D. Mitlin, Energy & Environmental Science, 8 (2015) 941-955.
[27] M.S. Dandekar, G. Arabale, K. Vijayamohanan, Journal of Power Sources, 141 (2005) 198-203.
[28] M. Galinski, K. Babeł, K. Jurewicz, Journal of Power Sources, 228 (2013) 83-88.
[29] W. Qiao, Y. Korai, I. Mochida, Y. Hori, T. Maeda, Carbon, 40 (2002) 351-358.
[30] S. Omokafe, A. Adeniyi, E. Igbafen, S. Oke, P. Olubambi, International Journal of Electrochemical Science, 15 (2020) 10854-10865.
[31] Y. Shao, F. Shen, Y. Shao, ChemElectroChem, 8 (2021) 484-491.
[32] L. Wang, Y. Zhang, H. Hu, H.-Y. Shi, Y. Song, D. Guo, X.-X. Liu, X. Sun, ACS Applied Materials & Interfaces, 11 (2019) 42000-42005.
[33] Y. Zhao, Z. Chen, F. Mo, D. Wang, Y. Guo, Z. Liu, X. Li, Q. Li, G. Liang, C. Zhi, Advanced Science, 8 (2021) 2002590.
[34] H. Wang, H. Zhang, Y. Cheng, K. Feng, X. Li, H. Zhang, Electrochimica Acta, 278 (2018) 279-289.
[35] N. Chang, T. Li, R. Li, S. Wang, Y. Yin, H. Zhang, X. Li, Energy & Environmental Science, 13 (2020) 3527-3535.
[36] Q. Nian, J. Wang, S. Liu, T. Sun, S. Zheng, Y. Zhang, Z. Tao, J. Chen, Angewandte Chemie International Edition, 58 (2019) 16994-16999.
[37] C. Lu, X. Chen, Nano Letters, 20 (2020) 1907-1914.
[38] J.J.P. Stewart, Journal of Computer-Aided Molecular Design, 4 (1990) 1-103.
[39] K.M. Dieter, J.J.P. Stewart, Journal of Molecular Structure: THEOCHEM, 163 (1988) 143-149.
[40] W. Humphrey, A. Dalke, K. Schulten, Journal of Molecular Graphics, 14 (1996) 33-38.
[41] K. Gunasekaran, R. Annadurai, P.S. Kumar, Construction and Building Materials, 28 (2012) 208-215.
[42] N.M. Keppetipola, M. Dissanayake, P. Dissanayake, B. Karunarathne, M.A. Dourges, D. Talaga, L. Servant, C. Olivier, T. Toupance, S. Uchida, K. Tennakone, G.R.A. Kumara, L. Cojocaru, RSC Advances, 11 (2021) 2854-2865.
[43] Y. Huang, Z. Li, S. Jin, S. Zhang, H. Wang, P. Hiralal, G.A.J. Amaratunga, H. Zhou, Carbon, 167 (2020) 431-438.
[44] R. Jiang, C. Cui, H. Ma, Electrochimica Acta, 104 (2013) 198-207.
[45] J. Jiang, S. I. Sandler, Industrial & Engineering Chemistry Research, 42 (2003) 6267-6272.
[46] Q. Nian, T. Sun, S. Liu, H. Du, X. Ren, Z. Tao, Chemical Engineering Journal, 423 (2021) 130253.
[47] F. Yue, Z. Tie, S. Deng, S. Wang, M. Yang, Z. Niu, Angewandte Chemie International Edition, 60 (2021) 13882-13886.
[48] J. S. Park, J. W. Park, E. Ruckenstein, Polymer, 42 (2001) 4271-4280.
[49] Y. Gogotsi, R.M. Penner, ACS Nano, 12 (2018) 2081-2083.
[50] V. Augustyn, P. Simon, B. Dunn, Energy & Environmental Science, 7 (2014)

1597-1614.
[51] H. Wang, M. Wang, Y. Tang, Energy Storage Materials, 13 (2018) 1-7.
[52] Z. Li, D. Chen, Y. An, C. Chen, L. Wu, Z. Chen, Y. Sun, X. Zhang, Energy Storage Materials, 28 (2020) 307-314.
[53] Y. Zhu, X. Ye, H. Jiang, J. Xia, Z. Yue, L. Wang, Z. Wan, C. Jia, X. Yao, Journal of Power Sources, 453 (2020) 227851.
[54] M. Maheswara, K.S.V.K. Rao, J.Y. Do, Tetrahedron Letters, 49 (2008) 1795-1800.
[55] J. S. Park, J. W. Park and E. Ruckenstein, Polymer, 2001, 42, 4271-4280
[56] J. Wang, F. Liu, F. Tao, Q. Pan, ACS Applied Materials & Interfaces, 9 (2017) 27745-27753.
[57] M. Wang, L. Fan, G. Qin, X. Hu, Y. Wang, C. Wang, J. Yang, Q. Chen, Journal of Membrane Science, 597 (2020) 117740.
[58] S. Xu, M. Zhang, G. Zhang, J. Liu, X. Liu, X. Zhang, D. Zhao, C. Xu, Y. Zhao, Journal of Power Sources, 441 (2019) 227220.
[59] T. Deng, W. Zhang, H. Zhang, W. Zheng, Energy Technology, 6 (2018) 605-612.
[60] L. Su, L. Gong, C. Ma, X. Wang, Z. Sun, ChemElectroChem, 4 (2017) 46-48.
[61] L. Su, L. Gong, X. Wang, H. Pan, International Journal of Energy Research, 40 (2016) 763-769.
[62] X. Li, L. Liu, X. Wang, Y.S. Ok, J.A.W. Elliott, S.X. Chang, H.-J. Chung, Scientific Reports, 7 (2017) 1685.
[63] J. Jiang, Journal of The Electrochemical Society, 164 (2017) H5043-H5048.
[64] M. Zhong, Q.F. Tang, Z.G. Qiu, W.P. Wang, X.Y. Chen, Z.J. Zhang, Journal of Energy Storage, 32 (2020) 101904.
[65] X. Lu, R.J. Jiménez-Riobóo, D. Leech, M.C. Gutiérrez, M.L. Ferrer, F. del Monte, ACS Applied Materials & Interfaces, 12 (2020) 29181-29193.
[66] H. Shim, Ö. Budak, V. Haug, M. Widmaier, V. Presser, Electrochimica Acta, 337 (2020) 135760.
[67] L. Ye, Q. Liang, Z. Huang, Y. Lei, C. Zhan, Y. Bai, H. Li, F. Kang, Q. Yang, Journal of Materials Chemistry A, 3 (2015) 18860-18866.
[68] P. Yang, C. Feng, Y. Liu, Advanced Energy Materials, 10 (2020) 2002898.
[69] R. Liu, Y. Peng, J. Cao, Polymer Composites, 37 (2016) 1971-1977.
[70] S.L. Bee, M.A.A. Abdullah, S.T. Bee, L.T. Sin, A.R. Rahmat, Progress in Polymer Science, 85 (2018) 57-82.
[71] A. Vasylieva, I. Doroshenko, Y. Vaskivskyi, Y. Chernolevska, V. Pogorelov, Journal of Molecular Structure, 1167 (2018) 232-238.

Graphical abstract

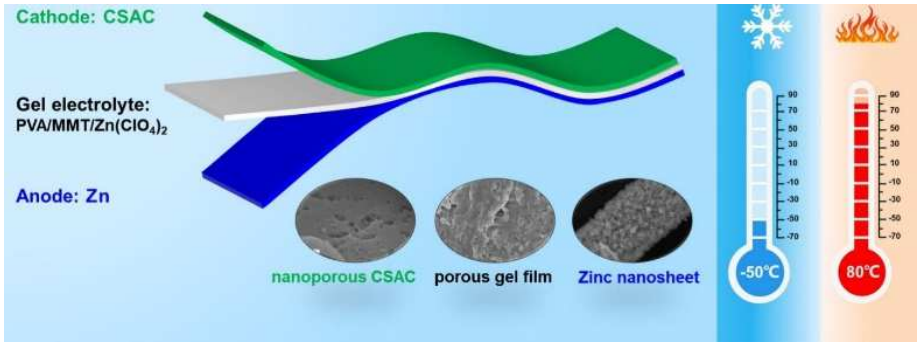

KEYWORDS: Biomass activated carbon; zinc perchlorate; wide temperature range; high energy density; zinc-ion hybrid supercapacitors

HIGHLIGHTS

- A natural biomass coconut shell derived nanoporous activated carbon is used as cathode.
- A low cost $Zn(ClO_4)_2$ aqueous electrolyte with superior anti-freezing property is revealed.
- The superior energy density and low cost of flexible ZHSC was manufactured.
- The flexible ZHSC delivers operate under a wide temperature range from -50 to 80 °C.

Author information

Guoshen Yang received his Ph.D. degree from the University of Yamanashi in 2019. Dr. Yang is currently a postdoctoral researcher at School of Electronic and Computer Engineering, Peking University Shenzhen Graduate School. His research recently focuses on energy storage and conversion applications including zinc ion batteries and supercapacitors.

Jialei Huang received his B.S. degree from Shaanxi University of Science & Technology. Then she received his master degree from Central South University. Now she is a research assistant at School of Electronic and Computer Engineering, Peking University Shenzhen Graduate School. Her research recently focuses on zinc ion batteries and metal corrosion.

Xuhao Wan joined in the School of Electrical Engineering and Automation, Wuhan University in 2019. He also received his B.S. in Wuhan University. His current research is mainly focused on single atom catalysts for electrochemical energy conversion reactions and the algorithms of DFT and machine learning hybrid scheme.

Yachao Zhu received his Ph.D. degree from the Université Paul Sabatier (Toulouse III) & Université de Montpellier in 2020. Dr. Zhu is currently a postdoctoral researcher at

L'Institut Charles Gerhardt Montpellier (ICGM). His research recently focuses on enhanced electric double-layer capacitor, advanced Pseudocapacitor and modified Water-in-salt electrolyte.

Binbin Liu received his B.S. degree from Sun Yat-sen University in 2019. Now he is a master candidate at School of Electronic and Computer Engineering, Peking University Shenzhen Graduate School. His research interests are energy storage devices, wearable electronics and system integration.

Jiawei Wang received his B.S. degree from Xidian University in 2019. Now he is a master candidate at School of Electronic and Computer Engineering, Peking University Shenzhen Graduate School. His research focuses on low-temperature flexible zinc-ion batteries.

Dr. Pritesh Hiralal, studied Physics at Manchester and completed his Ph.D. in Engineering at the University of Cambridge. He has spent time in business in Spain and set up Casa Hiralal S.L. and Zendal Backup. He has spent time in industry at the Nokia Research Centre working on high power energy storage, and has published 40+ papers and 15+ patents in the field. He has consulted for materials as well as energy storage device companies. He spent time as a Research Associate as well as an adjunct lecturer at the University of Cambridge. For the last 4 years he has co-founded and is the CTO of Zinergy, developing thin, flexible batteries which have gone from lab demonstrator all the way to production, entering the market in 2021.

Olivier Fontaine worked as a postdoctoral researcher at Collège de France, University of ST Andrews. He worked as a lecturer at the L'Institut Charles Gerhardt Montpellier. He is now an associate professor at Vidyasirimedhi Institute of Science and Technology (VISTEC) since 2020 in Thailand. His research interest is ionic liquid design and fundamental electrochemistry about supercapacitors and lithium-air batteries.

Yuzheng Guo is currently a professor in School of Electrical Engineering and Automation, Wuhan University. He obtained his Ph.D. degree in Engineering from Cambridge University. He has published more than 100 peer-reviewed journal papers. His research focuses on electronic materials and devices, computational methods, and energy materials. (For personal

reasons, Professor Guo does not want to disclose his personal portrait photo. If it is necessary, please contact us.)

Dr. Hang Zhou is currently an associate professor at Peking University Shenzhen Graduate School. He received his Ph.D. degree from University of Cambridge. He is now served as vice director of Shenzhen Thin Film Transistor and Advanced Display Lab. His research focuses on organic photodetectors, perovskite image sensors and flexible batteries. His lab is known for advancing the development of high energy density zinc ion batteries based on carbon nanomaterials enhanced electrodes and biopolymer electrolytes.

Cathode: CSAC

Gel electrolyte:
PVA/MMT/$Zn(ClO_4)_2$

Anode: Zn

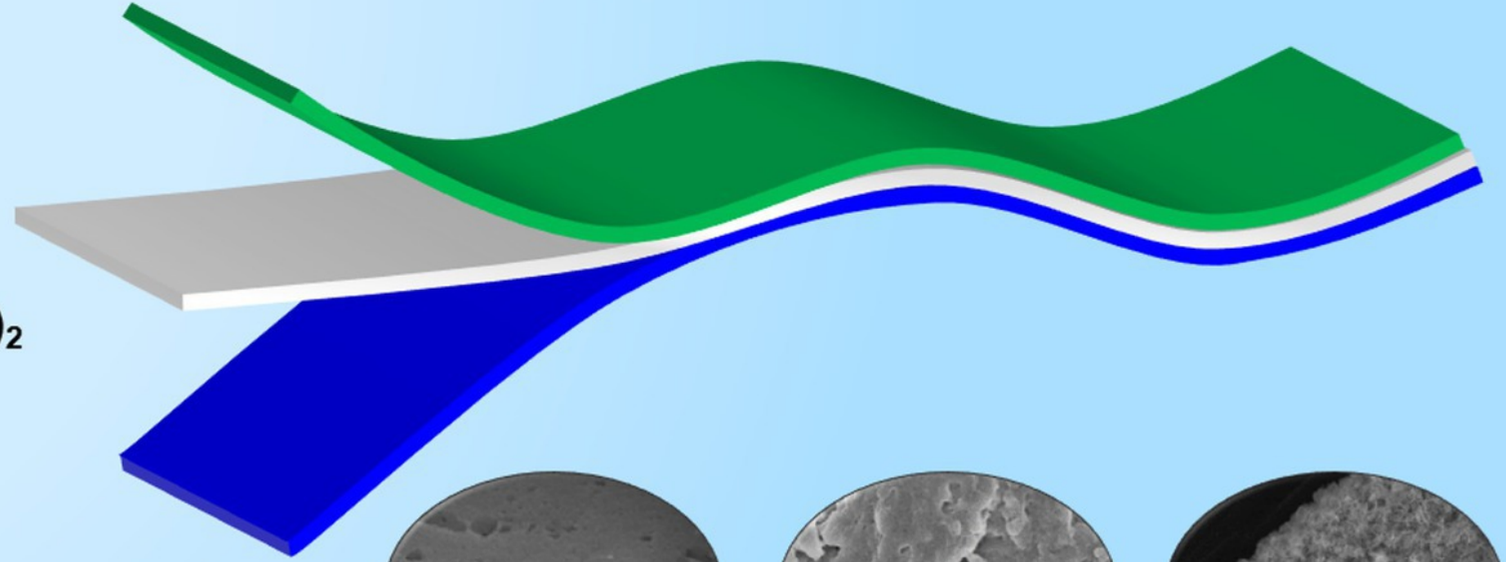

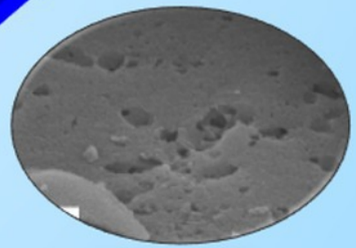

nanoporous CSAC

porous gel film

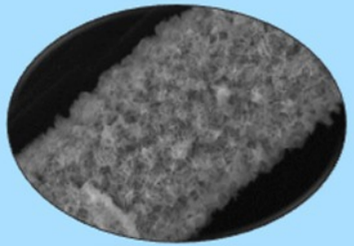

Zinc nanosheet